Asian Journal of Scientific Research

ISSN 1992-1454

science alert
http://www.scialert.net

ANSInet
an open access publisher
http://ansinet.com

OPEN ACCESS Asian Journal of Scientific Research

ISSN 1992-1454
DOI: 10.3923/ajsr.2016.24.33

Research Article
Microporous Activated Carbon Fiber from Pineapple Leaf Fiber by H_3PO_4 Activation

Sumrit Mopoung and Pornsawan Amornsakchai

Department of Chemistry, Faculty of Science, Naresuan University, Phitsanulok, 65000, Thailand

Abstract

Activated carbon fiber was prepared from pineapple fiber by carbonization followed with chemical activation using H_3PO_4. The activation was performed using a 1:1 w/v ratio of starting materials and H_3PO_4. Activated carbon fiber was also directly prepared by soaking pineapple fiber in H_3PO_4. The surface morphology and textural characteristics of activated carbon fibers vary with the activation temperature. The carbonized and activated products were characterized by SEM-EDS, FTIR, XRD and BET methods. The results for the activated products showed that the surface area, average pore size and percent micropore were increased as the activation temperature was increased from 400-600°C. The surface area of activated carbon fibers from pineapple fiber was 440.9211-636.3495 m^2 g^{-1}. Furthermore micropores (73.40-83.92%) are present in these activated products. It was shown that the activated carbon fibers prepared using pre-carbonization and phosphoric acid activation had higher BET surface area than materials prepared without nonpre-carbonization at the same activation temperature. However, the process without pre-carbonization uses less energy than other processes. The P-containing and O-containing surface functional groups were found on materials prepared using phosphoric acid activation, pineapple leaf fiber base activated carbon fiber by without pre-carbonization and pre-carbonization. Based on the results of this study it can be concluded that pineapple fiber is a suitable material for the preparation of adsorption filters.

Key words: Activated carbon fiber, pineapple leave fiber, phosphoric acid, microporous

Received: September 07, 2015 **Accepted:** October 08, 2015 **Published:** December 15, 2015

Citation: Sumrit Mopoung and Pornsawan Amornsakchai, 2016. Microporous Activated Carbon Fiber from Pineapple Leaf Fiber by H_3PO_4 Activation. Asian J. Sci. Res., 9: 24-33.

Corresponding Author: Sumrit Mopoung, Department of Chemistry, Faculty of Science, Naresuan University, Phitsanulok, 65000, Thailand

Competing Interest: The authors have declared that no competing interest exists.

Data Availability: All relevant data are within the paper and its supporting information files.

INTRODUCTION

Plant fibers are composed from cellulose, hemicelluloses and lignin. They also contain other minor components such as pectin, waxes and water-soluble substances, which are hydrophilic (Gurunathan *et al*., 2015). Thermochemical reactions viz., combustion and pyrolysis are important processes in the conversion of biomass from agricultural wastes into functional materials such as activated carbon fibers. Acid treatment during combustion and pyrolysis leaves a major impact, which affects the quality and properties of the resulting activated carbon fibers such as pore size, surface area and surface functional groups (Lee *et al*., 2014). Activated carbon fibers have a wide range of applications, including air purification, dehumidification and water purification as they possess large specific surface area, high adsorption capacity and rate and specific surface reactivity (Sim *et al*., 2014). Activated carbon fibers have also been used as active electrode material in supercapacitors (Diez *et al*., 2014). Phosphoric acid has been used as activation agent for activated carbon preparation. It functions both as an acid catalyst to promote bond cleavage reactions and formation of crosslinks and to combine with organic species to form phosphate and polyphosphate bridges that connect and crosslink polymer fragments (Chen *et al*., 2008). The pineapple leaf is also composed of holocellulose, alpha-cellulose and lignin (Van Tran, 2006). It has been used for fiber preparation (Yusof *et al*., 2015), plastic reinforcement (Kengkhetkit and Amornsakchai, 2014) and paper production (Laftah and Rahaman, 2015). Pineapple is grown in many countries worldwide, such as Brazil, Philippines, Costa Rica, Malaysia, Indonesia, Hawaii and Thailand on a land totaling about 2.1 million acres. After harvesting, a large amount of pineapple leaf waste, approximately 20,000-25,000 kg $acre^{-1}$, remains causing various problems for farmers (Kengkhetkit and Amornsakchai, 2014).

The aim of this study is to create microporous structure and surface chemical properties of pineapple leaf fiber based activated carbon fiber. The pyrolysis of pineapple leaf fiber in the presence of H_3PO_4 by 1 step (activation without pre-carbonization) and 2 steps (pre-carbonization followed with activation) were carried out. The effect of activation temperature (400-600°C) on the surface chemistry and porous texture of the resulting activated carbon fibers were investigated.

MATERIALS AND METHODS

Pineapple leaf fiber preparation: Pineapple Leaf Fiber (PALF) was collected from mechanical milling process. The fresh pineapple leaves, which contain approximately 80% water were chopped into pieces of 5-8 mm long. These were then wet-milled with a ball-mill or a disc mill. Milled material was cleaned with tap water to obtain PALF (Kengkhetkit and Amornsakchai, 2012). After that, PALF was oven (SL 1375 SHEL LAB 1350 FX) dried at 105°C for 6 h and then kept in a plastic bag.

Activated carbon fiber preparation

Non pre-carbonization activation method: Samples of PALFs were accurately weighed by analytical balance (Satorious Basci) and impregnated with 85% phosphoric acid (AR grade, Lab scan) in 1:1 w/v impregnation ratio. The impregnated mixtures were oven dried at 105°C for 1 day. The dried impregnated mixtures were then placed in a closed crucible (size 105/73, 102/70) and activated at 400, 500 and 600°C in an electric furnace (Fisher Scientific Isotemp® Muffle Furnace) under partial oxygen of atmosphere. The temperature was increased with a rate of 10°C min^{-1} up to the desired temperature and kept constant for 1 h. Finally, the activated carbon fibers were cooled to room temperature. The activated carbon fibers were washed with 0.2 M HCl (AR grade, Lab scan) and hot distilled water until pH ~7. After that the washed products were oven dried at 105°C for 1 day and then, kept in the desiccator with label PALFNPAC.

Pre-carbonization activation method: The activation with pre-carbonization or 2 step processing includes a first carbonization step followed by a second activation step.

- **Carbonization step:** The dried PALFs were carbonized at 500°C with temperature increased at a rate of 10°C min^{-1} and kept constant for 1 h. The carbon fibers obtained form PALF (PALFC) were used for activation in second step
- **Activation step:** The PALFCs were impregnated with 85% phosphoric acid using a 1:1 weight/volume impregnation ratio to achieve their activation. The impregnated mixtures were oven dried at 105°C for 1 day. The dried impregnated mixtures were activated as well as the samples prepared without pre-carbonization. The product of this step is labeled as PALFPAC. All PALFPACs were washed with 0.2 M HCl and then oven dried at 105°C for 3 h and kept in the desiccator

Analysis and characterization: The thermal behavior of the PALF was investigated as function of pyrolysis temperature in an O_2 combustion atmosphere with differential scanning calorimetry (DSC-1, Mettler) between room temperature and

800°C. The PALF was analyzed for proximate composition, including moisture (ASTM., 1996a), ash (ASTM., 1996b), volatile mater (ASTM., 1996c) and fixed carbon (ASTM., 1994). The lignin, cellulose and hemicellulose were determined following a report of Inari *et al*. (2007) and Zhang *et al*. (2015), respectively.

Instruments analyses: The PALF, PALFCs, PALFNPACs and PALFPACs were also characterized other instruments. Fourier transform infrared spectrometer (Spectrum GX, Perkin Elmer) in the range 4000-400 cm^{-1} was used for characterization of functional groups on surface of the all samples. The samples were prepared as pellets using KBr (Yang *et al*., 2011). An X-ray powder diffractometer with a Cu tube anode (PW 3040/60, X' Pert Pro MPD) was used to record the X-ray patterns of samples. Scanning electron microscopy (PHILIPS LEO 1455 VP) was used to visualize the surface morphology of the carbonized and activated products. The samples were coated with gold by a gold sputtering device for a clear vision of the surface morphology. Elemental composition of these samples was also determined using scanning electron microscopy equipped with energy dispersive spectrometer. The EDS spectra showing elemental composition were obtained by scanning through the surfaces of the samples. The surface distributions were collected from SEM pictures using different magnifications. Textural characteristics were determined by N_2 adsorption at -196°C on brunauer emmett teller surface area analyzer (Micromeritics TriStar II). The samples were degassed at 250°C for 12 h under vacuum before the measurements. The specific surface areas were estimated by the multipoint Brunauer Emmett Teller (BET) equation.

RESULTS AND DISCUSSION

Thermal behavior of PALF by TGA: Figure 1 shows the TGA curve of PALF from room temperature to 800°C. A weight loss of about 6% observed between room temperature and 120°C and a gradual weight loss between 120 and 260°C was assigned to evaporation of water vapour and the absorbed moisture (Li *et al*., 2015) of PALF. The first step weight loss took place in the temperature range 260-380°C and is attributed to oxidative pyrolytic decomposition of cellulose and hemicellulose and to partial lignin decomposition. Pyrolysis of hemicellulose and cellulose usually occurs rapidly in the range 200-300 and 300-400°C (Rosas *et al*., 2009) with about 70% weight loss, which corresponds to the amount of the hemicellulose and cellulose content of PALF. The lignin decomposition usually results in a gradual weight loss in the temperature range 380-680°C. Because of lignin has a chemical structure, which is more difficult to decompose in comparison to cellulose due to the presence of benzene rings (Lee *et al*., 2014). The second, minor and rapid weight loss took place in the temperature range 680-700°C and is attributed to oxidative pyrolytic decomposition of lignin and char. The very low weight (about 1.7%) of the final residue observed in the temperature range 700-800°C is mainly due to the complete oxidation of lignin and char with the presence of oxygen to produce combustion ash in the form of oxides (Lee *et al*., 2014). The amount of residue in this experiment corresponds to the amount of ash content of PALF.

Composition of PALF: The proximate composition of PALF is 4.81% moisture, 1.69% ash, 78.9% volatile matter and 14.6%

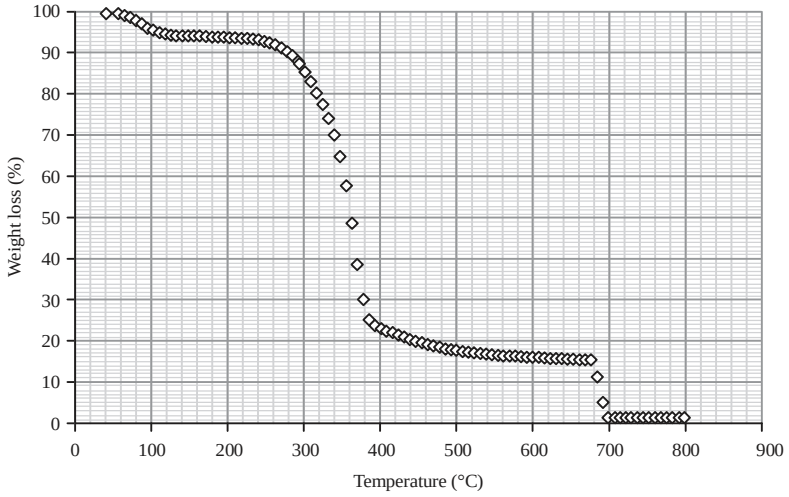

Fig. 1: TGA curve of PALF

Table 1: Elemental composition of PALF, PALFC, PALFNPACs and PALFPACs as a function of activation temperature determined by EDS analysis

	Element composition (wt %)					
Samples and temperature (°C)	C	O	Si	Ca	P	K
PALF	45.31±2.25	49.47±2.07	1.21±0.13	1.03±0.65	1.44±0.21	1.22±0.02
PALFC 500	73.16±3.27	21.04±3.01	1.81±0.27	1.35±1.34	2.01±0.12	1.35±0.03
PALFNPAC 400	54.31±4.02	31.28±2.34	2.09±1.26	1.19±1.02	10.86±0.52	0.86±0.05
PALFNPAC 500	57.67±3.21	29.02±2.35	2.43±1.42	1.63±1.02	10.09±0.76	0.76±0.02
PALFNPAC 600	62.53±2.52	24.93±2.36	2.41±0.35	0.55±0.02	12.56±0.32	0.71±0.01
PALFPAC 400	53.43±3.78	30.90±2.82	1.98±0.30	1.69±0.66	10.45±0.23	1.36±0.04
PALFPAC 500	55.18±4.02	33.09±2.34	2.08±1.26	0.30±0.01	8.77±0.54	0.48±0.01
PALFPAC 600	60.27±2.88	25.71±2.67	2.03±0.32	0.54±0.03	8.53±0.61	0.41±0.01

C: Carbon, O: Oxygen, P: Phosphorus, Ca: Calcium, K: Potassium and Si: Silicon group

fixed carbon. The organic composition of PALF is 1.98±0.08% lignin, 19.80±0.21% hemicellulose and 70.98±0.93% cellulose. These compositions are based on the results of TGA.

Elements composition of PALF, PALFC, PALFNPACs and PALFPACs: Table 1 shows the elemental composition of PALF, PALFC, PALFPACs and PALFPACs. It can be seen that content of all elements except oxygen, increased after carbonization and activation. This is due to the liberation of volatile compounds during the carbonization process (Avelar *et al*., 2010) and pyrolytic decomposition by phosphoric acid (Ren *et al*., 2011). Furthermore, these elements and compounds made from them are chemically stable and could survive extensive washing after carbonization or activation processes (Myglovets *et al*., 2014), except Ca and K. The content of phosphorous in the materials increases drastically after activation with phosphoric acid. This is due to the interaction of phosphoric with the carbon skeleton or organic material in the precursor materials leading to formation of phosphate linkages (Chen *et al*., 2008). Furthermore, carbon and phosphorous content of PALFNPACs are higher than in PALFPACs. This phenomenon is due to formation of more phosphate linkages with organic matter in PALF, as PALFC has low content of organic material. The changes in the content of O and P indicated the formation of surface functional groups containing oxygen and phosphorous (Li *et al*., 2015). Indeed, the carbon contents of activated samples are lower than of PALFC. The reason in this case is the catalytic effect of phosphoric acid leading to the decomposition of carbon by the bond cleavage reactions followed by the development of porous structures (Ren *et al*., 2011). It seems that PALFPACs may have higher pore volume than PALFNPACs obtained at the same activation temperature. This is because the carbon content of PALFPACs is decomposed to a higher degree than that of PALFNPACs.

FTIR spectra of PALF, PALFC, PALFNPACs and PALFPACs: The FTIR transmission spectra of PALF, PALFC, PALFNPACs and PALFPACs are shown in Fig. 2. Spectra of all samples exhibit broad bands between 3200 and 3600 cm^{-1} with maxima at about 3400 cm^{-1}, which can be assigned to the O-H stretching modes of hydroxyl groups and adsorbed water molecules (Lim *et al*., 2015). The intensities of these peaks decreased after carbonization and activation. This shows that water was thermally removed from PALF. The FTIR spectrum of PALF (Fig. 2a) shows a small band at around 2920 cm^{-1} due to the C-H stretching in methyl and methylene groups (Zheng *et al*., 2014). The peaks at 1710 and 1640 cm^{-1} are attributed to the stretching vibrations of C = O in ketones, carboxylic acids and the aromatic ring stretching vibrations (C = C) (Yang *et al*., 2011), respectively. The small peaks between 1500 and 900 cm^{-1} correspond to the functional groups of cellulose and lignin as described by Yang *et al*. (2011). These peaks disappeared after carbonization at 500°C (Fig. 2b). This shows that the volatile matters were thermally decomposed during the heating of PALF. One exception is the band between 3200 and 3600 cm^{-1} whose intensity decreases. The spectra of PALFC (Fig. 2b) contain new peaks at about 1720 and 1600 cm^{-1} due to C = O stretching vibrations in ketones, aldehydes and aromatic esters (Lim *et al*., 2015) and the C = O stretching in quinones (Yang *et al*., 2011), respectively. Both peaks are found in PALFNPACs and PALFPACs albeit with smaller intensity. This reveals that the presence of phosphoric acid can result in thermal decomposition and destruction of organic compounds in PALF and PALFC. Furthermore, the spectra of both PALFNPACs and PALFPACs exhibit more new peaks in around 1200 and 1000 cm^{-1}, which could be assigned to phosphate groups. The band at 1144-1154 cm^{-1} could be assigned to P = O groups of phosphates or polyphosphates, O-C stretching vibration in the P-O-C (aromatic) linkage, P = OOH and the symmetric stretching mode of O-P-O non-bridging oxygen atoms (Jha *et al*., 2015). The band at about 1000 cm^{-1} could be assigned to P-O-C asymmetric stretching, P-OH bending, interaction between aromatic ring vibration and P-C (aromatic) stretching, P-O-P asymmetric stretching in polyphosphates and symmetrical stretching

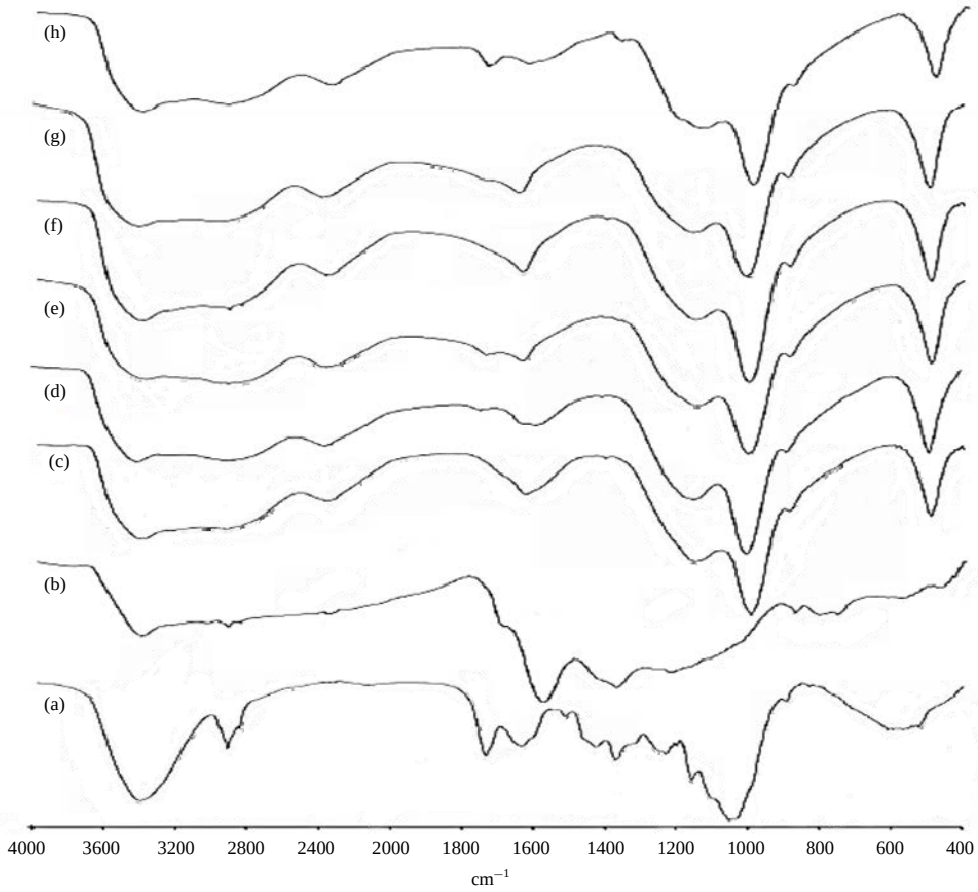

Fig. 2(a-h): Fourier transform infrared transmission spectra of, (a) PALF, (b) PALFC prepared at 500°C, (c) PALFNPAC prepared at 400°C, (d) PALFNPAC prepared at 500°C, (e) PALFNPAC prepared at 600°C, (f) PALFPAC prepared at 400°C, (g) PALFPAC prepared at 500°C and (h) PALFPAC prepared at 600°C

of PO_2 and PO_3 in phosphate-carbon complexes (Suarez-Garcia *et al*., 2004). The very weak peak at 887 cm^{-1} found in PALFC, PALFNPACs and PALFPACs, which appeared after carbonization and activation with H_3PO_4 is related to silanol groups (Si-O containing groups) (Guo and Rockstraw, 2007), which originated from raw PALF. This band can also be attributed to asymmetric stretching of P-O-P groups. It has been suggested that the phosphate group is built from short chains containing phosphorus-oxygen and pyrophosphate groups ($P_2O_7^{4-}$) (Jha *et al*., 2015). Another band at about 490 cm^{-1} found in all of the PALFNPACs and PALFPACs corresponds to P^+-O^- vibrations (Sych *et al*., 2012), which indicates the change of the pyrophosphate groups to orthophosphate groups (Jha *et al*., 2015). There is also a small band at 2348-2374 cm^{-1} in all PALFNPACs and PALFPACs, which corresponds to P-H vibrations (Abdelghany *et al*., 2014) and has higher intensity than in NFMCs. This result suggests that H_3PO_4 produces carbon oxidation, introducing oxygenated functionalities (Lim *et al*., 2015) in both PALFNPACs and PALFPACs.

XRD patterns of PALF, PALFC, PALFNPACs and PALFPACs: Figure 3 shows that the PALF (Fig. 3a) was composed of cellulose (2* = 16.5, 22.5 and 34.5°) (Benitez-Guerrero *et al*., 2014) and lignin (2* = 22°) (Vivekanand *et al*., 2014). After carbonization at 500°C, there are no cellulose and lignin peaks in PALFC (Fig. 3b). However, there are 2 new broad peaks at 24 and 43° which were assigned to disordered carbon structures (Jin *et al*., 2014). PALFC also contains a sharp peak at 29.5° and a small peak at 34.5° which were attributed to a calcium compound (Tianxue *et al*., 2014) and a potassium compound (Diaz-Teran *et al*., 2003), respectively. Furthermore, it had a little peak at 23°, which corresponds to silica (Guo and Rockstraw, 2007). This silica originates from raw PALF. It has also remained in PALFNPACs and PALFPACs, in which the corresponding peak had higher intensity because silica is

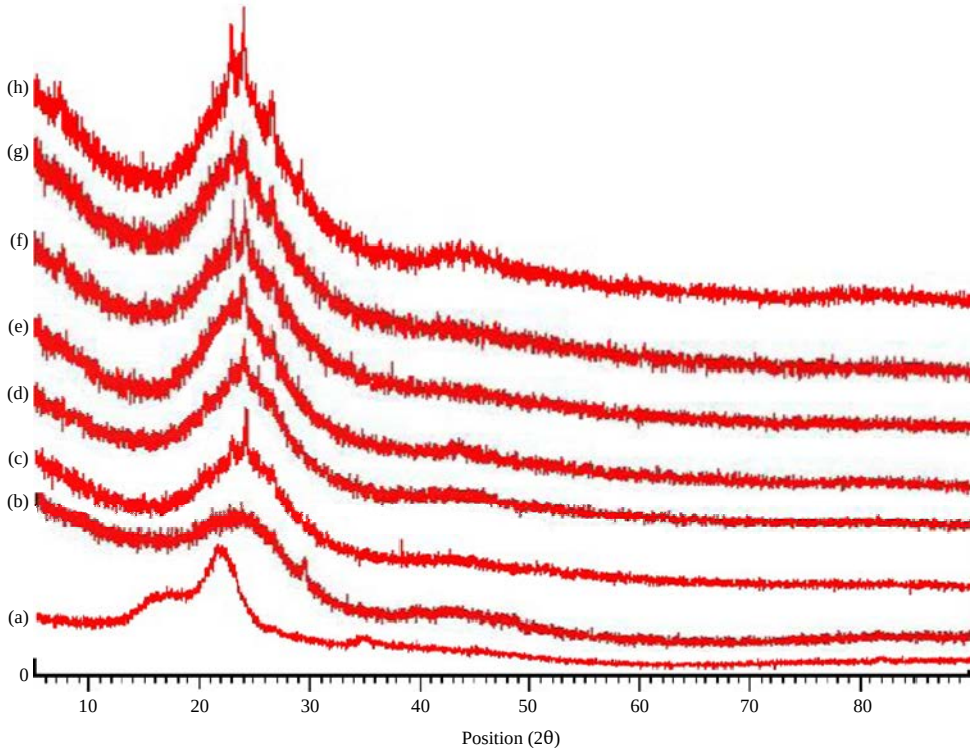

Fig. 3(a-h): X-ray diffractograms of, (a) PALF, (b) PALFC prepared at 500°C, (c) PALFNPAC prepared at 400°C, (d) PALFNPAC prepared at 500°C, (e) PALFNPAC prepared at 600°C, (f) PALFPAC prepared at 400°C, (g) PALFPAC prepared at 500°C and (h) PALFPAC prepared at 600°C

thermally stable (Guo and Rockstraw, 2007). For activated materials, the new sharp peak at about 24° in both PALFNPACs and PALFPACs was attributed to P-C (Zhu *et al*., 2015). It was confirmed that phosphoric acid interacted with the carbon skeleton or organic material of PALF and PALFC and then formed of phosphate linkages (Ren *et al*., 2011) on the PALFNPACs and PALFPACs surface. It was seen that the intensity of silica peaks (23°) of PALFPACs are higher than those of PALFNPACs. This is because of the phosphate content of PALFNPACs is higher than that of PALFPACs. This resulted in the dominant phosphate peaks and depressed the peak intensity of silica as well as the intensity of peaks of potassium and calcium compounds in PALFNPACs.

SEM morphology: Figure 4 shows SEM images of PALF (a) and PALFC carbonized at 500°C. The raw PALF (Fig. 4a) exhibits highly packed bundles with some pits and holes on the surface. However, the PALFC obtained using carbonization at 500°C had a groove form with parallel streak ridges that follow the longitudinal fibers. It is the result of thermal degradation of volatile matter (Shcherban *et al*., 2014). The degradation of volatile matter at 500°C is attributed to the evaporation of the surface moisture and volatilization of cellulose and hemicellulose and partial lignin decomposition followed by densification and contraction (Lee *et al*., 2014). It is also attributable to the collapse of aromatic rings (skeletal carbon) (Yang *et al*., 2011).

After activation with phosphoric acid at temperature of 400-600°C, the PALFNPACs and PALFPACs were spread to sub fibers (Fig. 5a-f). This has shown that PALF consisted of many sub dense fibers, which formed by bond cleavage reactions and crosslinking (Chen *et al*., 2008) caused by the phosphoric acid. Both PALFNPACs and PALFPACs are more broken and contracted, which is attributed to more extensive dehydration and thermal decomposition of organic compounds or carbon (Castro-Muniz *et al*., 2011). This effect is the cause of the destruction of the morphology (Romero-Anaya *et al*., 2012) in both PALFPACs and PALFPACs. Furthermore, the PALFPACs are more broken and contracted than PALFNPACs. This result suggests that the porosity of PALFC after carbonization is more than that of raw PALF and thus phosphoric acid could penetrate deeper into the texture of PALFC. Therefore, the polymeric chains of PALFC are broken and have reacted with phosphoric acid forming phosphate

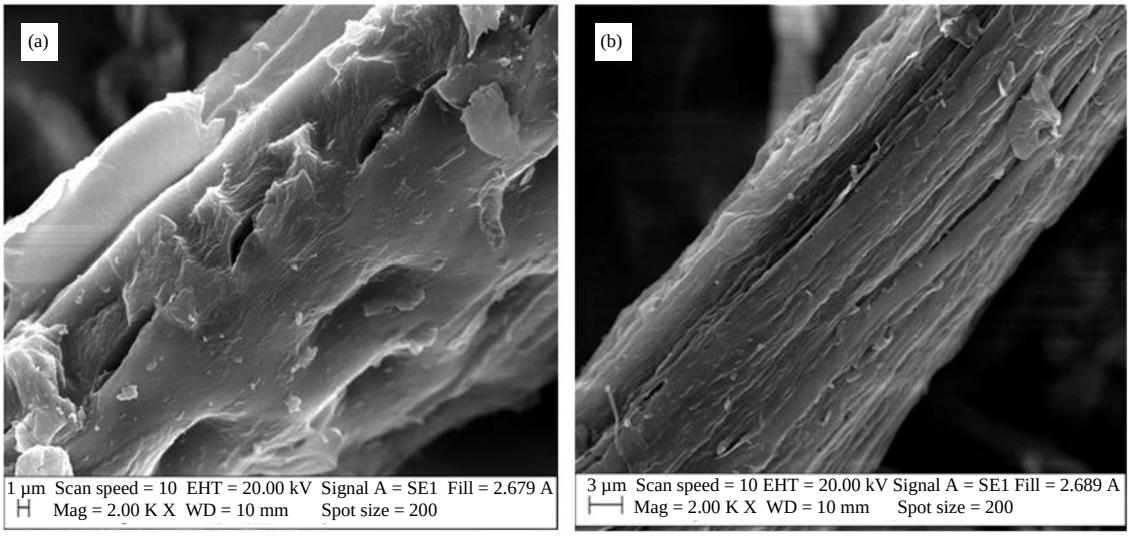

Fig. 4(a-b): Scanning electron microscope micrographs of (a) PALF and (b) PALFC prepared at 500°C

Table 2: Brunauere Emmett teller surface area, pore volume, pore size and percent micropore of PALF, PALFC, PALFNPAC and PALFPAC as function of activation temperature

Samples and temperature (°C)	BET surface area (m^2 g^{-1})	Pore volume (cm^3 g^{-1})	Average pore size (nm)	Micropore (%)
PALF	3.1318	0.00347	4.4316	-
PALFC 500	21.6120	0.01782	9.0308	-
PALFNPAC 400	4.8082	0.00630	1.9413	74.27
PALFNPAC 500	440.9211	0.21637	1.9476	78.83
PALFNPAC 600	445.6875	0.21297	5.2435	83.92
PALFPAC 400	294.2739	0.11257	3.2983	73.40
PALFPAC 500	534.3411	0.25933	1.9413	77.59
PALFPAC 600	636.3495	0.30984	1.9238	76.80

BET: Brunauere Emmett teller

and polyphosphate bridges. This in turn resulted in the porosity, which was created up PALFC degradation (Suárez-Garcı'a *et al*., 2004).

Textural characteristics of PALF, PALFC, PALFNPACs and PALFPACs are shown in Table 2. It was shown that the PALFC obtained by carbonization at 500°C has surface area, pore volume and average pore size higher than PALF. This is the result of the evolution of compounds produced from the cross linking reactions and shrinkage in the material (Yang *et al*., 2011), which is consistent with the results of SEM imaging (Fig. 4). It was also shown that PALFNPACs and PALFPACs exhibit a strictly microporous structure with a high contribution of micropores (73.40-83.92%), which is also evident from the SEM micrographs (Fig. 5). It was shown that phosphoric acid is crucial for the micropore formation in activated carbon materials. In addition, the BET surface area, pore volume and percent of micropore of PALFNPACs and PALFPACs are likely to increase with increasing activation temperature from 400-600°C. It was shown that the amorphous carbon is removed from the network by reactions between carbon and phosphoric acid, which causes the change of pore structure and texture characteristics (Zheng *et al*., 2014). This is because the polymeric chains are broken and react with phosphoric acid forming phosphate and polyphosphate bridges (Castro-Muniz *et al*., 2011). These phosphate and polyphosphate bridges become thermally unstable at temperatures above 500°C and promote the development of micropores (Chen *et al*., 2008). However, the average pore size of PALFNPACs increases with increasing activation temperature, while the trend in pore size of PALFPACs is inversed. The percent of micropores in PALFNPACs tends to be higher than in PALFPACs. This is because the addition of H_3PO_4 to the PALF accelerates the dehydration of the cellulose and promotes inflame retarding and crosslinking. Thus, it could be proposed that the proportion of micropores increases at the same time while the meso/macropore sizes grow (Chen *et al*., 2008). Indeed, it was observed that the PALFNPACs, which were obtained after

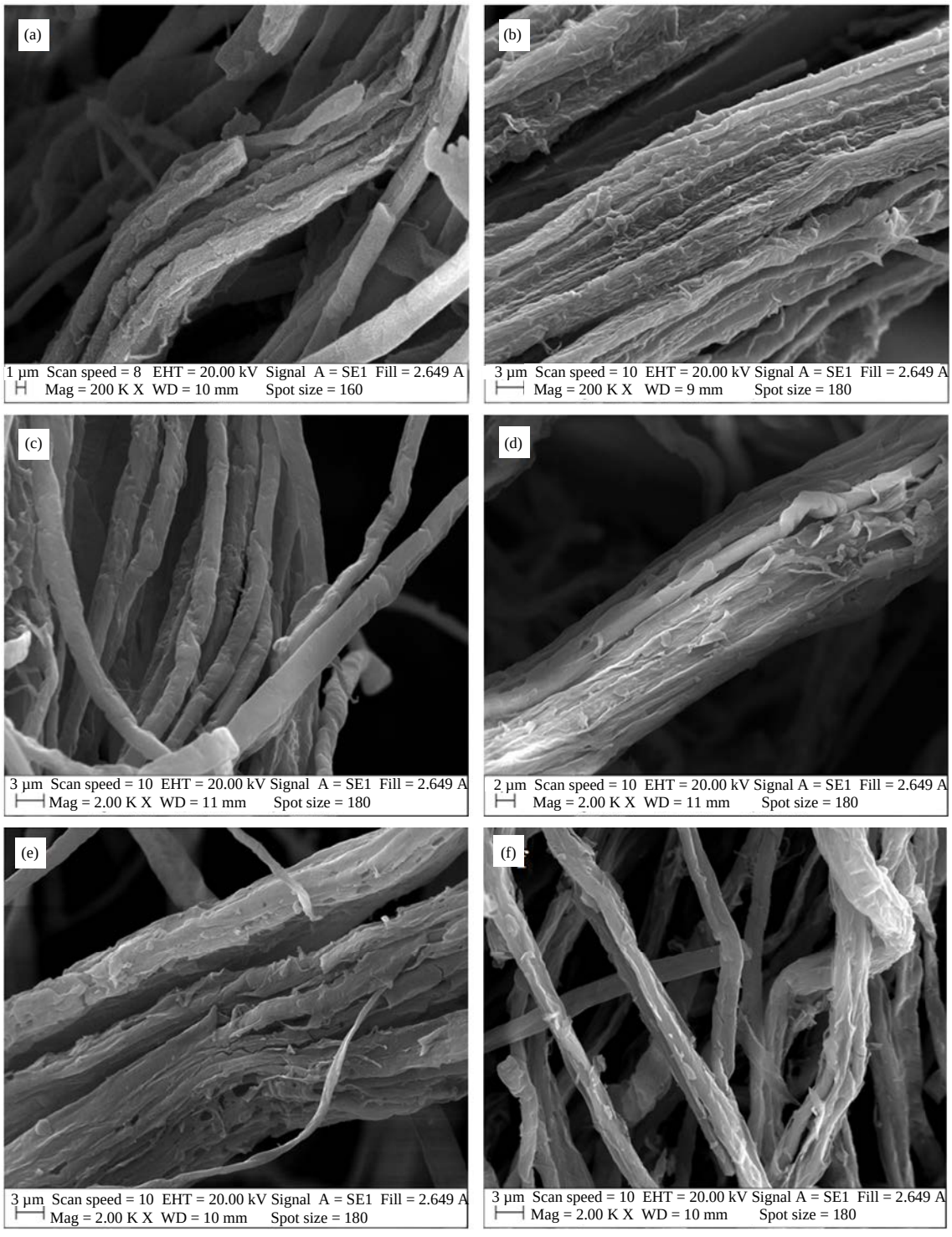

Fig. 5(a-f): Scanning electron microscope micrographs of (a) PALFNPAC prepared at 400°C, (b) PALFNPAC prepared at 500°C, (c) PALFNPAC prepared at 600°C, (d) PALFPAC prepared at 400°C, (e) PALFPAC prepared at 500°C and (f) PALFPAC prepared at 600°C

activation at 400°C, have BET surface area, pore volume and average pore size lower than PALFC, which were carbonized at 500°C. This observation could be explained by the phosphoric acid, which dehydrates the material during

activation, remaining as salts of phosphoric acid inside the porous structure of the activated carbon occupying substantial volumes. Another reason is the rupture of phosphate and polyphosphate bridges, which takes place prior volatilization leading to bond breakdown and contraction in the material. This is reflected in a decrease in the volume of micropores (Suarez-Garcia *et al*., 2004), which can be seen in Fig. 4b and 5a. Furthermore, as when a comparison of textural characteristics of PALFNPACs and PALFPACs is made, the values of BET surface area and pore volume of PALFNPACs are lower than of PALFPACs obtained at the same activation temperature. This is because the polymeric chains of PALFC, which was carbonized at 500°C, were broken and have reacted with phosphoric acid forming phosphate and polyphosphate bridges. Thus, the porosities are formed after PALFC degradation as a result of phosphoric acid withdrawal or P-compound volatilization, which keeps the carbonaceous material structure expanded (Castro-Muniz *et al*., 2011).

CONCLUSION

It can be concluded that phosphoric acid has a strong effect on the textural structures of activated carbon fibers from pineapple leaf fiber, especially on the micropores. This conclusion is supported by the results of FTIR, XRD, SEM-EDS and BET surface area analysis, which are all in good agreement. Furthermore, it has been shown that the activated carbon fibers obtained after pre-carbonization followed with phosphoric activation had higher BET surface area, average pore size and percent of micropores than materials prepared without pre-carbonization. However, the pore volume and percent of micropores are reverse as same activation temperature. However, the process without pre-carbonizatio uses less energy than the process including pre-carbonization followed by activation process. In addition, the BET surface area, pore volume, average pore size and percent of micropores in activated products have increased with increasing activation temperatures. The only exception is the average pore size of PALFPACs, which show a reverse trend. Furthermore, the P-containing and O-containing surface functional groups are formed after phosphoric acid activation in both PALFNPACs and PALFPACs, which can also affect adsorption properties. Thus, it is possible to prepare activated carbon fibers for the production of adsorption filter from PALF.

ACKNOWLEDGMENT

This study was financially supported by National Research Council of Thailand. The authors acknowledge Science Lab Center, Faculty of Science, Naresuan University for all of the analysis.

REFERENCES

ASTM., 1994. Standard test method for fixed carbon in activate carbon. ASTM D 3172-89, American Standard of Testing Material (ASTM), USA.

ASTM., 1996a. Standard test method for moisture in activate carbon. ASTM D 2867-95, American Standard of Testing Material (ASTM), USA.

ASTM., 1996b. Standard test method for total ash content of activate carbon. ASTM D 2866-94, American Standard of Testing Material (ASTM), USA.

ASTM., 1996c. Standard test method for volatile matter content of activate carbon. ASTM D 5832-95, American Standard of Testing Material (ASTM), USA.

Abdelghany, A.M., F.H. ElBatal, H.A. ElBatal and F.M. EzzElDin, 2014. Optical and FTIR structural studies of CoO-doped sodium borate, sodium silicate and sodium phosphate glasses and effects of gamma irradiation-a comparative study. J. Mol. Struct., 1074: 503-510.

Avelar, F.F., M.L. Bianchi, M. Goncalves and E.G. da Mota, 2010. The use of piassava fibers (*Attalea funifera*) in the preparation of activated carbon. Bioresour. Technol., 101: 4639-4645.

Benitez-Guerrero, M., J. Lopez-Beceiro, P.E. Sanchez-Jimenez and J. Pascual-Cosp, 2014. Comparison of thermal behavior of natural and hot-washed sisal fibers based on their main components: Cellulose, xylan and lignin. TG-FTIR analysis of volatile products. Thermochimica Acta, 581: 70-86.

Castro-Muniz, A., F. Suarez-Garcia, A. Martinez-Alonso and J.M.D. Tascon, 2011. Activated carbon fibers with a high content of surface functional groups by phosphoric acid activation of PPTA. J. Colloid Interface Sci., 361: 307-315.

Chen, Y., Q. Wu, P. Ning, G. Jinghua and P. Ding, 2008. Rayon-based activated carbon fibers treated with both alkali metal salt and lewis acid. Microporous Mesoporous Mater., 109: 138-146.

Diaz-Teran, J., D.M. Nevskaia, J.L.G. Fierro, A.J. Lopez-Peinado and A. Jerez, 2003. Study of chemical activation process of a lignocellulosic material with KOH by XPS and XRD. Microporous Mesoporous Mater., 60: 173-181.

Diez, N., P. Diaz, P. Alvarez, Z. Gonzalez and M. Granda *et al*., 2014. Activated carbon fibers prepared directly from stabilized fibers for use as electrodes in supercapacitors. Mater. Lett., 136: 214-217.

Guo, Y. and D.A. Rockstraw, 2007. Activated carbons prepared from rice hull by one-step phosphoric acid activation. Micropor. Mesopor. Mater., 100: 12-19.

Gurunathan, T., S. Mohanty and S.K. Nayak, 2015. A review of the recent developments in biocomposites based on natural fibres and their application perspectives. Compos. Part A: Applied Sci. Manuf., 77: 1-25.

Inari, G.N., S. Mounguengui, S. Dumarcay, M. Petrissans and P. Gerardin, 2007. Evidence of char formation during wood heat treatment by mild pyrolysis. Polym. Degrad. Stabil., 92: 997-1002.

Jha, P.K., O.P. Pandey and K. Singh, 2015. FTIR spectral analysis and mechanical properties of sodium phosphate glass-ceramics. J. Mol. Struct., 1083: 278-285.

Jin, J., B.J. Yu, Z.Q. Shi, C.Y. Wang and C.B. Chong, 2014. Lignin-based electrospun carbon nanofibrous webs as free-standing and binder-free electrodes for sodium ion batteries. J. Power Sources, 272: 800-807.

Kengkhetkit, N. and T. Amornsakchai, 2012. Utilisation of pineapple leaf waste for plastic reinforcement: 1. A novel extraction method for short pineapple leaf fiber. Ind. Crop. Prod., 40: 55-61.

Kengkhetkit, N. and T. Amornsakchai, 2014. A new approach to Greening plastic composites using pineapple leaf waste for performance and cost effectiveness. Mater. Des., 55: 292-299.

Laftah, W.A. and W.A.W.A. Rahaman, 2015. Chemical pulping of waste pineapple leaves fiber for kraft paper production. J. Mater. Res. Technol., 4: 254-261.

Lee, T., Z.A. Zubir, F.M. Jamil, A. Matsumoto and F.Y. Yeoh, 2014. Combustion and pyrolysis of activated carbon fibre from oil palm empty fruit bunch fibre assisted through chemical activation with acid treatment. J. Anal. Applied Pyrol., 110: 408-418.

Li, J., D.H.L. Ng, P. Song, C. Kong, Y. Song and P. Yang, 2015. Preparation and characterization of high-surface-area activated carbon fibers from silkworm cocoon waste for congo red adsorption. Biomass Bioenergy, 75: 189-200.

Lim, W.C., C. Srinivasakannan and A. Al Shoaibi, 2015. Cleaner production of porous carbon from palm shells through recovery and reuse of phosphoric acid. J. Cleaner Prod., 102: 501-511.

Myglovets, M., O.I. Poddubnaya, O. Sevastyanova, M.E. Lindstrom and B. Gawdzik *et al*., 2014. Preparation of carbon adsorbents from lignosulfonate by phosphoric acid activation for the adsorption of metal ions. Carbon, 80: 771-783.

Ren, L., J. Zhang, Y. Li and C. Zhang, 2011. Preparation and evaluation of cattail fiber-based activated carbon for 2,4-dichlorophenol and 2,4,6-trichlorophenol removal. Chem. Eng. J., 168: 553-561.

Romero-Anaya, A.J., M.A. Lillo-Rodenas, C.S.M. de Lecea and A. Linares-Solano, 2012. Hydrothermal and conventional H_3PO_4 activation of two natural bio-fibers. Carbon, 50: 3158-3169.

Rosas, J.M., J. Bedia, J. Rodriguez-Mirasol and T. Cordero, 2009. HEMP-derived activated carbon fibers by chemical activation with phosphoric acid. Fuel, 88: 19-26.

Shcherban, N.D., P.S. Yaremov, V.G. Ilyin and M.V. Ovcharova, 2014. Influence of the method of activation on the structural and sorption properties of the products of carbonization of sucrose. J. Anal. Applied Pyrol., 107: 155-164.

Sim, K.M., K.H. Kim, G.B. Hwang, S.C. Seo, G.N. Bae and J.H. Jung, 2014. Development and evaluation of antimicrobial activated carbon fiber filters using *Sophora flavescens* nanoparticles. Sci. Total Environ., 493: 291-297.

Suarez-Garcia, F., A. Martinez-Alonso and J.M.D. Tascon, 2004. Nomex polyaramid as a precursor for activated carbon fibres by phosphoric acid activation. Temperature and time effects. Microporous Mesoporous Mater., 75: 73-80.

Sych, N.V., S.I. Trofymenko, O.I. Poddubnaya, M.M. Tsyba, V.I. Sapsay, D.O. Klymchuk and A.M. Puziy, 2012. Porous structure and surface chemistry of phosphoric acid activated carbon from corncob. Applied Surf. Sci., 261: 75-82.

Tianxue, Y., Y. Li, H. Haobo, X. Beidou and H. Liansheng *et al*., 2014. Spatial structure characteristic analysis of corn stover during alkali and biological co-pretreatment using XRD. Bioresour. Technol., 163: 356-359.

Van Tran, A., 2006. Chemical analysis and pulping study of pineapple crown leaves. Ind. Crops Prod., 24: 66-74.

Vivekanand, V., A. Chawade, M. Larsson, A. Larsson and O. Olsson, 2014. Identification and qualitative characterization of high and low lignin lines from an oat TILLING population. Ind. Crops Prod., 59: 1-8.

Yang, R., G. Liu, X. Xu, M. Li, J. Zhang and X. Hao, 2011. Surface texture, chemistry and adsorption properties of acid blue 9 of hemp (*Cannabis sativa* L.) bast-based activated carbon fibers prepared by phosphoric acid activation. Biomass Bioenergy, 35: 437-445.

Yusof, Y., S.A. Yahya and A. Adam, 2015. Novel technology for sustainable pineapple leaf fibers productions. Procedia CIRP, 26: 756-760.

Zhang, P., S.J. Dong, H.H. Ma, B.X. Zhang, Y.F. Wang and X.M. Hu, 2015. Fractionation of corn stover into cellulose, hemicellulose and lignin using a series of ionic liquids. Ind. Crops Prod., 76: 688-696.

Zheng, J., Q. Zhao and Z. Ye, 2014. Preparation and characterization of Activated Carbon Fiber (ACF) from cotton woven waste. Applied Surf. Sci., 299: 86-91.

Zhu, J., G. He, L. Liang, Q. Wan and P.K. Shen, 2015. Direct anchoring of platinum nanoparticles on nitrogen and phosphorus-dual-doped carbon nanotube arrays for oxygen reduction reaction. Electrochimica Acta, 158: 374-382.